Scattering of a Dirac electron on a mass barrier

A. Matulis,[1,2,*] M. Ramezani Masir,[1,†] and F. M. Peeters[1,‡]
[1]*Departement Fysica, Universiteit Antwerpen Groenenborgerlaan 171, B-2020 Antwerpen, Belgium*
[2]*Semiconductor Physics Institute, Center of Physical Sciences and Technology, Goštauto 11, LT-01108 Vilnius, Lithuania*
(Received 24 May 2012; published 1 August 2012)

The interaction of a wave packet (and in particular the wave front) with a mass barrier is investigated in one dimension. We discuss the main features of the wave packet that are inherent to two-dimensional wave packets, such as compression during reflection, penetration in the case when the energy is lower than the height of the barrier, waving tails, precursors, and the retardation of the reflected and penetrated wave packets. These features depend on the wave-packet envelope function which we demonstrate by considering the case of a rectangular wave packet with sharp front and trailing edges and a smooth Gaussian wave packet. The method of Fourier integral for obtaining the nonstationary solutions is used.

DOI: 10.1103/PhysRevA.86.022101 PACS number(s): 03.65.Pm, 73.22.−f, 73.63.Fg

I. INTRODUCTION

Progress in nanotechnology has triggered a broad interest in low dimensional physics. The separation of graphene by mechanical exfoliation in 2004 [1,2] opened a broad range of activity for theoretical and experimental researchers. The interest rose due to the peculiar properties of graphene such as ultrarelativistic behavior of charge carriers with a Fermi velocity 300 times smaller than the velocity of light, the linear spectrum close to K and K' points in the momentum plane that can be described by the massless Dirac-Weyl equation [1,3], an unconventional quantum Hall effect [4], and the perfect transmission through arbitrarily high and wide barriers, the so-called Klein tunneling [5].

The energy levels or the spectrum of the electron system typically investigated as being the main characteristics of quantum nanostructures (such as quantum dots) are found by considering the stationary Schrödinger equation [6]. Recently, a scientific interest has shifted to the investigation of quantum dynamics including quasibound states [7], electron beams, wave packets, and their control by means of barriers and other nonhomogeneous structures [8–10]. Unfortunately, due to the above-mentioned Klein effect and the gapless spectrum the control of electrons in graphene by means of electric fields is inefficient. Therefore, the search for other possibilities to control electrons in graphene becomes of interest. Recently, the creation of a gap in the electron spectrum [11] as well as the control of the valley isospin [12,13] was predicted by introducing a mass term into the Dirac-Weyl Hamiltonian. This possibility was experimentally demonstrated by the proper arrangement of dopants in the graphene sheet [14] or by inducing electron-electron interactions [15]. Therefore, the investigation of the nonstationary solutions of the Dirac equation describing the interaction of electrons with mass barriers becomes timely. Such sophisticated systems and problems are a challenge for numerical simulation. But in order to obtain a physical understanding of the behavior of such systems it is very helpful to invent and analyze simple models that are able to demonstrate the main physical features of interest.

The purpose of the present work is to demonstrate the mean properties of wave packets, such as their reflection and penetration into mass steps and barriers, the appearance of precursors, the formation of evanescent waves, and the *Zitterbewegung*, using very simple analytically solvable one-dimensional (1D) models. Comparing the results obtained for a rectangular wave packet with the ones having a rather soft Gaussian shaped wave packet we demonstrate that their propagation depends on the shape of the wave packet. In our analysis we pay special attention to the appearance of so-called precursors that were predicted by Sommerfeld nearly 100 years ago for electromagnetic waves traveling in a dispersive media [16]. We also focus on the waving after-effects that can be related to the *Zitterbewegung* that was predicted by Schrödinger for relativistic electrons [17] and which we predict should be observable in graphene [18]. The results were obtained applying the Fourier integral technique for solving the nonstationary Dirac equation and analyzing the solution by means of integration in the complex wave-vector plane.

The paper is organized as follows. In Sec. II we introduce the problem and the method of its solution considering the reflection of the Dirac wave packet from a hard wall. In Sec. III results for scattering of a plane-wave type wave function by the mass barrier are discussed, which enables us to present the nonstationary solutions for the reflected front in the form of a complex integral in Sec. IV. The penetration of the front of the wave packet into the barrier is considered in Sec. V, and in Sec. VI the scattering of the rectangular wave packet is studied. Section VII is devoted to the description of the scattering of a Gaussian wave packet. Our conclusions are presented in Sec. VIII.

II. REFLECTION OF A WAVE PACKET FROM A HARD WALL

We consider the motion of a 1D wave packet that is described by the following Dirac-Weyl equation:

$$i\frac{\partial}{\partial t}\Psi(x,t) = -i\sigma_x\frac{\partial}{\partial x}\Psi(x,t) + \Theta(x)\sigma_z\Psi(x,t), \qquad (1)$$

*amatulis@takas.lt
†mrmphys@gmail.com
‡francois.peeters@ua.ac.be

 ©2012 American Physical Society

where σ_x and σ_z are the Pauli matrices and the symbol $\Theta(x)$ stands for the Heaviside step function whose value is zero for negative argument and unity for the positive one. The last term will be referred to as the mass term, that leads to a gap in the electron spectrum close to the K and K' points.

In order to simplify the notations in the above equation, the results are presented in dimensionless notations based on the height of the mass barrier V. So, the energy is measured in V units, the time is measured in $\hbar/V$ units, and the unit of length is $\hbar v_F/V$, where the symbol v_F stands for the Fermi velocity. For the sake of illustration we took $V = 53$ meV, what is achieved by depositing the single graphene layer on a boron nitride substrate [19]. Then the time unit is a hundredth of a ps, and the unit of length is about 10 nm.

Presenting the wave function as a two component spinor

$$\Psi(x,t) = \begin{pmatrix} u(x,t) \\ v(x,t) \end{pmatrix} \tag{2}$$

we have to solve the following set of two differential equations for the wave-function components:

$$u_t = -v_x - 1\Theta(x)u, \tag{3a}$$

$$v_t = -u_x + 1\Theta(x)v. \tag{3b}$$

Apart from the wave-function components themselves the wave packet can be characterized by the local density

$$\rho(x,t) = |u(x,t)|^2 + |v(x,t)|^2, \tag{4}$$

the local current

$$j(x,t) = 2\mathrm{Re}\,[u^*(x,t)v(x,t)], \tag{5}$$

and some averaged values: the number of particles in the wave packet (the norm of the wave function)

$$N(t) = \int_{-\infty}^{\infty} dx\rho(x,t), \tag{6}$$

the mean position

$$X(t) = N^{-1}(t)\int_{-\infty}^{\infty} dx x\rho(x,t), \tag{7}$$

the mean velocity

$$V(t) = N^{-1}(t)\int_{-\infty}^{\infty} dx j(x,t), \tag{8}$$

and the width of the wave packet

$$w(t) = N^{-1}(t)\int_{-\infty}^{\infty} dx\,[x - X(t)]^2\,\rho(x,t). \tag{9}$$

In order to introduce the necessary definitions and illustrate the method of solving the time dependent Dirac equation we start with the most simple problem: the reflection of the wave packet from a hard wall. This means that Eq. (3) without the last term (i.e., the massless Dirac equation) will be solved in the negative part of the x axis ($-\infty < x \leqslant 0$) and the hard wall will be taken into account by the boundary condition

$$u(0,t) + iv(0,t) = 0 \tag{10}$$

which was derived and discussed in Ref. [13].

This solution can be easily composed of two (incident and reflected) freely propagating wave packets. The incident wave packet moving to the right side can be presented as

$$\Psi^{(\mathrm{in})}(x,t) = \frac{1}{\sqrt{2}}\begin{pmatrix} 1 \\ 1 \end{pmatrix} e^{iq(x-t)}\Phi(t-x), \tag{11}$$

that satisfies the above massless equation with any envelope function $\Phi(x)$. In order to satisfy the boundary condition Eq. (10) at any time t we have to add the reflected wave packet

$$\Psi^{(\mathrm{rfl})}(x,t) = \frac{-i}{\sqrt{2}}\begin{pmatrix} 1 \\ -1 \end{pmatrix} e^{-iq(x+t)}\Phi(t+x), \tag{12}$$

that propagates to the left.

The most interesting feature of the wave function constructed in such a way as

$$\Psi(x,t) = \Psi^{(\mathrm{in})}(x,t) + \Psi^{(\mathrm{rfl})}(x,t), \tag{13}$$

and describing the Dirac electron reflection from the hard wall is the absence of the interference of the incident and reflected wave packets. Indeed, denoting

$$f_{\pm} = e^{iq(\pm x - t)}\Phi(t \mp x), \tag{14}$$

we present the density as

$$\begin{aligned}\rho(x,t) &= |f_+ - if_-|^2 + |f_+ + if_-|^2 \\ &= |f_+|^2 + |f_-|^2 = |\Phi(t-x)|^2 + |\Phi(t+x)|^2\end{aligned} \tag{15}$$

and the current as

$$\begin{aligned}j(x,t) &= \mathrm{Re}\{(f_+^* + if_-^*)(f_+ + if_-)\} \\ &= \mathrm{Re}\{|f^+|^2 - |f^-|^2 + 2i\mathrm{Re}(f_+^* f_-)\} \\ &= |f^+|^2 - |f^-|^2 = |\Phi(t-x)|^2 - |\Phi(t+x)|^2.\end{aligned} \tag{16}$$

Thus, the density and current are expressed just through the corresponding individual values of the incident and reflected wave packets without any interference terms.

In order to trace how the reflection depends on the form of the envelope function we consider in detail two extreme shapes of wave packets: a wave packet with a rectangular envelope as an example of a wave packet with abrupt edges and a rather soft Gaussian one.

We choose the following envelope for the rectangular wave packet:

$$\Phi(x) = \frac{1}{a}\Theta(a^2/4 - x^2). \tag{17}$$

Inserting this into Eqs. (7)–(9) we obtain the following mean values:

$$X(t) = -|t|\Theta\left(t^2 - \frac{a^2}{4}\right) - \frac{4t^2 + a^2}{4a}\Theta\left(\frac{a^2}{4} - t^2\right), \tag{18a}$$

$$V(t) = -\frac{t}{|t|}\Theta\left(t^2 - \frac{a^2}{4}\right) - \frac{2t}{a}\Theta\left(\frac{a^2}{4} - t^2\right), \tag{18b}$$

$$w(t) = \frac{a^2}{12} - \left(\frac{4t^2 - a^2}{4a}\right)^2\Theta\left(\frac{a^2}{4} - t^2\right), \tag{18c}$$

characterizing the reflection of the rectangular wave packet from the hard wall. They are shown in Fig. 1(a). We would like to draw the reader's attention to the following features

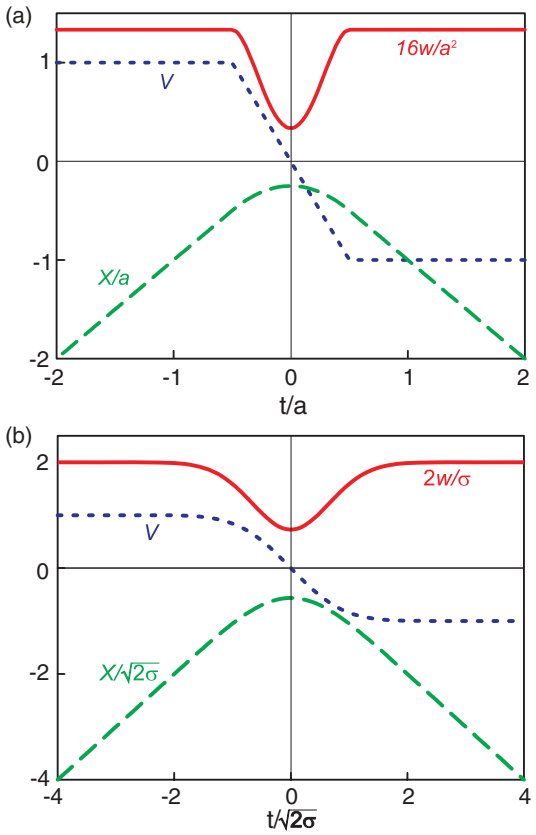

FIG. 1. (Color online) Evolution of mean values for the Dirac wave packet in time: the mean coordinate of the wave packet (green dashed curve), the mean velocity (blue dotted curve), and the width (red solid curve). (a) Rectangular wave packet with envelope Eq. (17) and (b) the Gaussian one with envelope Eq. (19).

of this simple example of reflection: (1) the wave packet is reflected before it reaches the wall, (2) it is compressed during the reflection, and (3) its dimensions are restored after the reflection. This behavior can be compared with the one of a rubber ball hitting a hard wall: due to its finite extension the ball changes the direction of motion before its center reaches the wall and it is squeezed during the collision.

In the case of a Gaussian wave packet the following envelope function was chosen:

$$\Phi(x) = \frac{e^{iqx}}{(2\pi\sigma)^{1/4}} e^{-x^2/4\sigma}, \tag{19}$$

where the parameter σ characterizes the width of the wave packet and plays the same role as the parameter a in the previous case of a rectangular wave packet. Now inserting this expression into Eqs. (11)–(13) and then into Eqs. (7)–(9) we obtain the following averaged values:

$$X(t) = -\sqrt{\frac{2\sigma}{\pi}} e^{-t^2/2\sigma} - t\,\mathrm{erf}(t/\sqrt{2\sigma}), \tag{20a}$$

$$V(t) = -\mathrm{erf}(t/\sqrt{2\sigma}), \tag{20b}$$

$$w(t) = \sigma + t^2 - \left[\sqrt{\frac{2\sigma}{\pi}} e^{-t^2/2\sigma} - t\,\mathrm{erf}(t/\sqrt{2\sigma})\right]^2, \tag{20c}$$

where the symbol erf stands for the error function. These dependencies are shown in Fig. 1(b). Comparing Figs. 1(a) and 1(b) we see that qualitatively they are the same, and consequently the reflection of the Dirac wave packet from the infinite wall is not sensitive to the form of the envelope function. This nonsensitivity is quite expected because the dispersionless propagation of the wave packet described by Eq. (1) without the mass term is not spoiled by the dispersionless boundary condition Eq. (10).

III. MASS BARRIER OF A FINITE HEIGHT

Now we consider our main problem: the interaction of a wave packet with a mass barrier of finite height. This problem is much more complicated than the previous one because now the wave packet spends some time inside the barrier region which is a dispersive medium, and as a consequence the wave packet will not conserve its shape.

As the Dirac equation is linear with coordinate independent coefficients a natural way to solve the problem is by using Fourier transformation. Thus, we choose the initial condition (say the position of the wave packet at time $t = 0$), expand it into Fourier series (here integral over momentum k), and then change the exponent in the integrand by the function that obeys the time dependent Dirac equation in both regions (the barrier and free motion region) and is consistent with the boundary conditions at the point $x = 0$. For this purpose we recap briefly the main results for scattering of a plane-wave (exponent) type wave function.

We assume that in the region of free motion ($-\infty < x < 0$) there are incident and reflected waves with energy $\varepsilon = k$, and here the total wave function reads

$$\Psi^{(\mathrm{free})}(x,t) = \Psi^{(\mathrm{in})}(x,t) + \Psi^{(\mathrm{rfl})}(x,t) = \frac{1}{\sqrt{2}}\left\{\begin{pmatrix}1\\1\end{pmatrix} e^{ikx} + R\begin{pmatrix}1\\-1\end{pmatrix} e^{-ikx}\right\} e^{-ikt}. \tag{21}$$

In the barrier region ($0 < x < \infty$) there is only an outgoing wave moving to the right with the same energy k and momentum $\kappa = \sqrt{k^2 - 1}$. We present its wave function as

$$\Psi^{(\mathrm{tr})}(x,t) = \frac{T}{\sqrt{2k}}\begin{pmatrix}\sqrt{k+1}\\ \sqrt{k-1}\end{pmatrix} e^{i\kappa x} e^{-ikt}. \tag{22}$$

Now equating both wave-function components at the point $x = 0$ we obtain the following wave reflection and penetration amplitudes:

$$R(k) = k - \kappa, \tag{23a}$$

$$T(k) = \sqrt{k}(\sqrt{k+1} - \sqrt{k-1}). \tag{23b}$$

Equations (21) and (22) together with definitions Eq. (23) enable us to present the time dependent wave function of any wave packet in the form of the integral along some contour in the complex k plane.

IV. REFLECTION OF A STEEP FRONT

First we consider the motion of the wave packet with the rectangular envelope function. Fortunately, due to the linearity of the Dirac equation this problem can be decomposed into

the motion of two fronts corresponding to the leading and trailing edges of this wave packet. That is why we start with the reflection of a steep front from the mass barrier and choose the initial incident wave packet as

$$\Psi^{(\mathrm{inc})}(x,0) = \frac{1}{\sqrt{2}}\begin{pmatrix}1\\1\end{pmatrix} e^{iqx}\Theta(-x). \tag{24}$$

It coincides with the freely propagating front where the leading edge has reached the barrier. This function can be presented by the following Fourier integral:

$$\Psi^{(\mathrm{inc})}(x,0) = \frac{1}{\sqrt{2}}\begin{pmatrix}1\\1\end{pmatrix}\frac{1}{2\pi}\int_{-\infty}^{\infty} dk e^{ikx} f(k), \tag{25}$$

where

$$f(k) = \int_{-\infty}^{0} dx e^{[i(q-k)+\alpha]x} = \frac{1}{i(q-k)+\alpha}. \tag{26}$$

Here the symbol α stands for the regularization parameter—a small positive value that will be set to zero at the end of the calculation.

Now according to our strategy we replace the exponent $\exp(ikx)$ in the integrand of the Fourier integral (25) by the solution of the time dependent Dirac equations (21) and (22) describing the reflection and penetration into the barrier of this exponent type wave function. The wave function of the wave packet obtained in this way consists of three parts. Two of them are defined in the free motion region ($-\infty < x < 0$) and describe the incident front

$$\Psi^{(\mathrm{in})}(x,t) = -\frac{1}{\sqrt{2}}\begin{pmatrix}1\\1\end{pmatrix}\frac{1}{2}\int_C \frac{dk e^{ik(x-t)}}{k-q+i\alpha} \tag{27}$$

and the reflected one

$$\Psi^{(\mathrm{rfl})}(x,t) = -\frac{1}{\sqrt{2}}\begin{pmatrix}1\\-1\end{pmatrix}\frac{1}{2}\int_C \frac{e^{-ik(x+t)}(k-\kappa)dk}{k-q+i\alpha}. \tag{28}$$

The third part of the wave function is defined in the region $0 < x < \infty$ and describes the front that penetrates the barrier:

$$\Psi^{(\mathrm{tr})}(x,t) = -\frac{1}{2^{3/2}}\int_C \frac{e^{i(\kappa x-kt)}dk}{k-q+i\alpha}\begin{pmatrix}k+1-\kappa\\ \kappa-k+1\end{pmatrix}. \tag{29}$$

Equation (27) is trivial because its integrand has just a single singular point in the lower part of the complex k plane, namely, the pole at the point $k = q - i\alpha$. Thus, choosing the integration contour C by passing that point from above and enclosing it by the upper or lower semicircle (depending on the sign of the parameter $x - t$ in the exponent) we calculate the residue at this pole and obtain the following wave function of the incident front:

$$\Psi^{(\mathrm{in})}(x,t) = \frac{1}{\sqrt{2}}\begin{pmatrix}1\\1\end{pmatrix}\Theta(t-x)e^{iq(x-t)}, \tag{30}$$

that describes the motion of this front with a constant velocity equal to unity due to the absence of dispersion in the free motion region.

The two other integrals Eqs. (28) and (29) are more complicated because of the radicals $\kappa = \sqrt{k^2-1}$ in their integrands leading to branching points at $k_\pm = \pm 1$ in the complex k plane. Consequently, we have to make a cut in this plane and choose the position of the integration contour accordingly. How this is done by taking the causality principle into account is shown in Fig. 2(a). The choice of the Riemann sheet is defined by the requirement $\mathrm{Im}\,\kappa > 0$ in the upper half plane, and this is determined by the fact that at large momentum k (positive or negative) the value of κ should approximately coincide with the value of k. The choice of the integration contour C laying above both singularities (pole and cut) is in agreement with the requirement that the integral Eq. (28) should be zero in the case of $x < -t$ as the reflected front cannot move faster than with unit velocity.

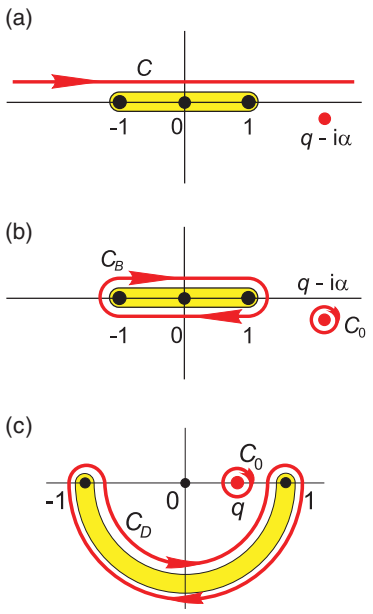

FIG. 2. (Color online) The complex k plane, pole, cut, and contour for the integration in Eqs. (28) and (29): (a) initial contour, (b) transformation of the contour in the case $q > 1$, and (c) transformation of the contour in the case $q < 1$.

In the case of $x > -t$ the argument of the exponent has the opposite sign and that is why the contour can be enclosed by the lower semicircle and transformed into two contours encircling the singularities as is shown in Figs. 2(b) and 2(c), corresponding to the contributions of pole and cut.

The pole contribution is calculated by means of the residue technique and it gives

$$\Phi^{(\mathrm{rfl})}_{\mathrm{pole}}(x,t) = \Theta(x+t)R(q)e^{-iq(x+t)}\frac{1}{\sqrt{2}}\begin{pmatrix}1\\-1\end{pmatrix}. \tag{31}$$

It coincides with the result presented in Sec. III for scattering of a plane wave. The single difference is that now the exponent has a steep leading edge.

The calculation of the cut contribution is more complicated. It cannot be calculated analytically, and a numerical evaluation of the integral is necessary. This integral depends essentially on the energy $\varepsilon = q$ of the incident front, namely, whether it is larger or smaller than the height of the barrier.

A. Above the barrier reflection ($q > 1$)

For $q > 1$ the contours C_0 and C_B are separated horizontally [see Fig. 2(b)] and the pole of the integrand does not complicate the calculation of the cut contribution along the contour C_B. That is why we transformed this contribution

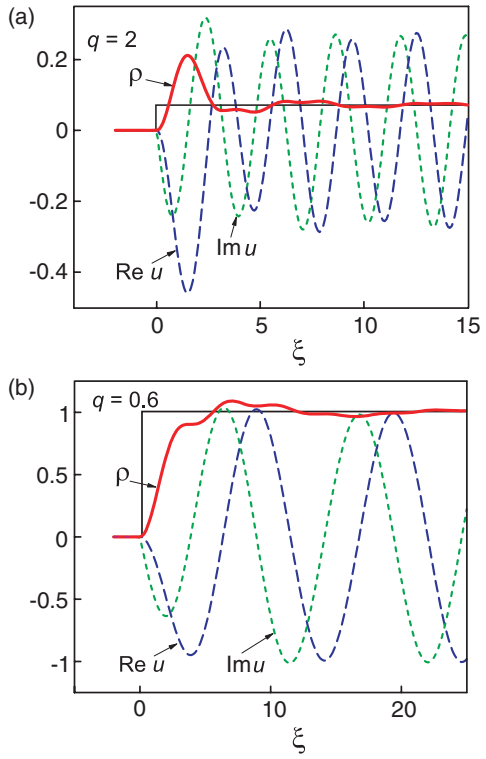

FIG. 3. (Color online) The wave function of the reflected front as a function of the variable $\xi = x + t$: the real part of the component $u = -v$ (blue dashed curve), the imaginary part of it (green dotted curve), the local density (red thick solid curve), and the same local density with only the pole contribution included (black thin solid curve). (a) Above the barrier reflection with energy $q = 2$. (b) Below the barrier reflection with $q = 0.6$.

into two real integrals that depend on the single argument $\xi = x + t$,

$$\Phi^{(\mathrm{rfl})}_{\mathrm{cut}}(x,t) \equiv \Phi^{(\mathrm{rfl})}_{\mathrm{cut}}(\xi) = -\frac{2}{\pi}\int_0^1 dk \frac{\sqrt{1-k^2}}{q^2-k^2}\{-q\cos(k\xi) + i\sin(k\xi)\}, \tag{32}$$

and integrated this numerically.

A typical result is shown in Fig. 3(a). There are two points worth mentioning. First, at the beginning of the front there is some overshoot of the wave-function modulus squared (the local density) as compared with the one when only the pole contribution is taken into account (as was already mentioned the pole contribution coincides with the result of plane-wave scattering). Second, the above-mentioned local density tends to the pole contribution with increasing $\xi = x + t$ (when we are going away from the leading edge of the front) but notice that some oscillations are still present. Following [10] the overshoot can be explained as follows. According to Fourier transform Eq. (27) the incident front can be considered as a superposition of numerous plane waves with energies larger and smaller than the height of the barrier whose interaction with the barrier can be examined independently due to above-mentioned linearity of the problem. In spite of the fact that the mean energy of the front q is larger than the height of the barrier, the plane waves in the above superposition with energy less than the barrier height are completely reflected and this reflection results in the above-mentioned overshoot. Next, we see the oscillating after-effect in the local density of the reflected front [see the thick red curve in Fig. 3(a)] that slowly tends to the pole contribution with increasing of ξ shown by the thin black steplike curve. Comparing definitions (4) and (5) and having in mind that both reflected wave components differ only by sign ($v = -u$) we conclude that the same oscillations are present in the current density as well. This after-effect is closely related to the *Zitterbewegung* [9]. Usually this trembling motion of the electron is explained by means of interference between positive- and negative-energy relativistic wave-function components. The interference itself is not sufficient and some additional perturbation is necessary. In our case this is the dispersive mass barrier that mixes the eigenfunctions of the free-electron motion. Compare with the reflection from the infinite barrier described in Sec. II where these components were not mixed.

B. Below the barrier reflection ($q < 1$)

If the front energy is lower than the height of the barrier some problem with the cut contribution appears because the pole is located exactly in the interval $-1 < x < 1$ and interferes with the integration contour C_B that is shown in Fig. 2(b). Therefore, we changed the cut and transformed the above integration contour into the C_D as shown in Fig. 2(c). The pole contribution gives the same result as in Eq. (31). Calculating the cut contribution as the integral along the C_D contour we changed the integration variable $k = \exp[i(\pi + \varphi)]$ in Eq. (28), presented this integral as

$$\Phi^{(\mathrm{rfl})}_{\mathrm{cut}}(\xi) = -\frac{\sqrt{2}}{\pi}\int_0^{\pi/2} d\varphi\sqrt{\cos\varphi}e^{-\xi\cos\varphi} \times\left[\frac{e^{i(3\varphi/2-\xi\sin\varphi)}}{q+ie^{i\varphi}} + \frac{e^{-i(3\varphi/2-\xi\sin\varphi)}}{q+ie^{-i\varphi}}\right], \tag{33}$$

and calculated this integral numerically. A typical result is shown in Fig. 3(b).

Comparing the curves in both Figs. 3(a) and 3(b) we note some differences. In the case of the below barrier reflection instead of an overshoot in the red thick solid curve that corresponds to the leading edge we see some diminishing of the electron density. This can be explained by the same superposition of many Fourier harmonics as in the previous above the barrier reflection case. Among them there are harmonics with energy larger than the barrier height. They do not reflect but penetrate the barrier that finally causes the above-mentioned lack of density at the reflected front.

V. PENETRATION INTO THE BARRIER

The calculation of the front part that penetrates the barrier is similar to the calculation of the reflected one presented in the previous sections. The only difference is that the integral Eq. (28) now is replaced by the integral Eq. (29). It leads to the different wave-function components that depend on both (x and t) arguments.

Calculating the integral Eq. (29) along the same contours in the complex k plane shown in Figs. 2(a) and 2(b) we divide

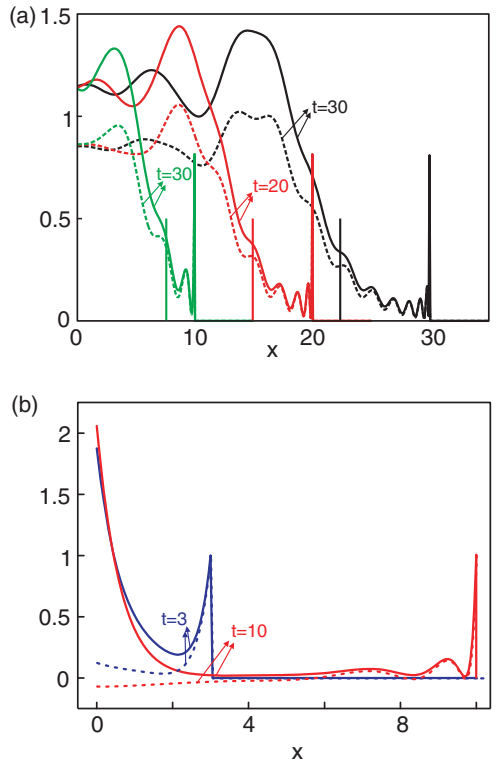

FIG. 4. (Color online) The local density [Eq. (4), solid curves] and current [Eq. (5), dotted curves] in the front that penetrate the barrier for different time t values. The thin vertical lines indicate the motion with the group velocity $x = v_{\rm gr}t$. (a) Above barrier reflection with $q = 1.5$. (b) Below barrier reflection with $q = 0.6$.

this contribution into two parts. As in the case of reflection the pole contribution is trivial:

$$\Psi^{(\rm tr)}_{\rm pole}(x,t) = \frac{\Theta(t-x)T(q)}{\sqrt{2q}} \begin{pmatrix} \sqrt{q+1} \\ \sqrt{q-1} \end{pmatrix} e^{ix\sqrt{q^2-1}} e^{-ikt}. \quad (34)$$

It represents the result obtained by the scattering of plane waves truncated at the point $x = t$ due to the finite velocity of the front.

The contribution of the cut was calculated using the formulas analogous to Eqs. (32) and (33) depending on whether the energy of the front is larger or smaller than the height of the barrier.

A. Above the barrier penetration ($q > 1$)

A typical result for the penetration of the front into the barrier with energy larger than the height of the barrier is shown in Fig. 4(a). The local density and current are shown as functions of the coordinate x in the case of different time t values. As was already pointed out the barrier acts as a dispersive medium. That is why the form of the front is not conserved, and the local density (actually the modulus of the wave function squared) and the current demonstrate a rather sophisticated behavior. Three important points are worth mentioning. First, the leading edge of the front is transformed into a sharp peak that moves with unit velocity inherent to the front in the dispersionless free motion region ($x < 0$). In the case of electromagnetic pulses it is known as a precursor [16]. The physical explanation of its appearance is as follows. The theory of dispersion in the classical [20] and quantum [21] version, and the mechanical analogy of the Klein-Gordon equation [22] as well, implies that the medium in which the waves propagate has its own degrees of freedom that actually causes the dispersion of waves in a stationary regime. This stationary regime corresponds to the excited state of the medium and, consequently, needs some time to be established. That is why the first piece of the front (the precursor itself) moves through the unexcited medium and does not undergo any dispersion. Speaking figuratively one can imagine that the precursor prepares the media for the propagation of the main part of the pulse or front. In an analogous way one may consider the mass barrier region as a medium with inner degrees of freedom whose quantum analog is the difference of the ground-state energies of the two sublattices when we consider the graphene in the tight-binding approximation. Consequently, the precursor has to be present in our Dirac electron case.

Second, as seen in Fig. 4(a) the main part of the front is retarded with respect to the above precursor. It carries the energy of the front, which is the reason why it moves with the group velocity $v_{\rm gr} = d\varepsilon/dq = \sqrt{q^2-1}/q$. In the case of $q = 1.5$ we have $v_{\rm gr} \approx 0.75$, which is indicated by thin vertical lines in Fig. 4(a).

And at last the third point is that in spite of the homogeneous barrier region we see the waving behavior far from the leading edge of the local density and current that are related to the above-mentioned *Zitterbewegung* and which is much more pronounced in the penetrated front.

B. Below the barrier penetration ($q < 1$)

A typical result is shown in Fig. 4(b) for the case of below barrier penetration when the front energy is lower than the height of the barrier.

Here again we see the precursor moving with unit velocity that makes the below the barrier reflection analogous to the above the barrier one. But now instead of preparing the barrier for the wave propagation this precursor constructs step by step the evanescent wave that is inherent to the under the barrier reflection of plane waves. This process needs some resources. That is why the precursor loses its intensity (becomes narrower during its motion) in contrast to the penetration with the energy larger than the height of the barrier where such losses are not noticeable [compare the precursors in Figs. 4(a) and 4(b)]. The oscillatory behavior of the penetrated fronts are also seen in the local density and current. This is in agreement with the fact that the mass barrier is a dispersive medium.

VI. PENETRATION OF THE RECTANGULAR WAVE PACKET INTO THE MASS BARRIER

The reflection and penetration of the steep fronts considered in the previous sections enable us to construct the result for the rectangular wave-packet reflection by the mass barrier. The result is obtained as the superposition of two fronts with the proper shift Δ and amplitudes chosen. The most interesting case is the below the barrier reflection that is shown in Fig. 5 in the case of $q = 0.9$. The reflected wave packet is shown

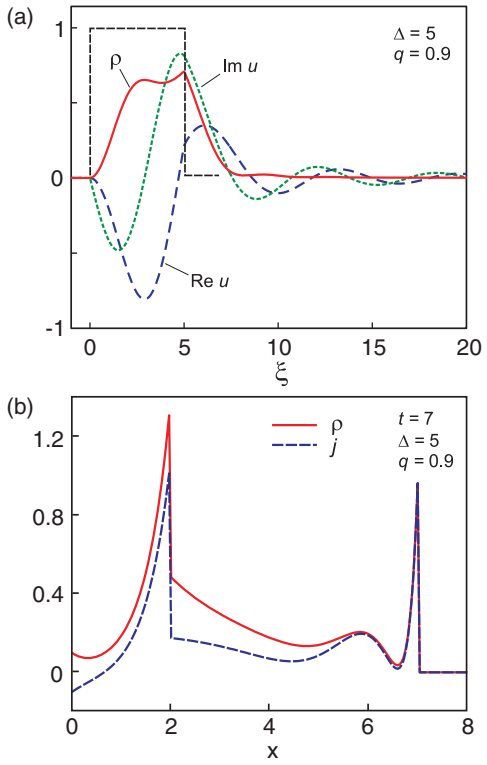

FIG. 5. (Color online) (a) Reflected rectangular wave packet with shift $\Delta = 5$ between the opposite fronts as a function of $\xi = x + t$: the real (blue dashed curve) and imaginary (green dotted curve) wave-function components and the local density (red solid curve); black dashed rectangular shows the wave packet reflected by a hard wall. (b) Local density (solid curves) and current (dotted curves) for the penetrated part of the wave packet, at a given time.

in Fig. 5(a). It depends on the argument $\xi = x + t$ as in the case of the front considered in the previous sections. The part of the wave packet that penetrates the barrier is a function of both x and t arguments. The local density is shown as a function of x in Fig. 5(b) for given time $t = 7$ (red solid curve) together with the current (blue dashed curve). Here we see two precursors. One of them constructs the evanescent wave, introducing some charge into the barrier, and later the other one destroys it, extracting that charge out of the barrier region. The part of that evanescent wave is clearly seen between those precursors. It is interesting to establish whether all charge is extracted or some of it is left in the barrier and continues its motion towards $+\infty$.

The easiest way to clear this point up is to compare the density in the reflected wave packet [the red solid curve in Fig. 5(a)] with the black dashed curve in the same figure that represents the wave packet reflected by the hard wall. It is evident that the area below the red solid curve is smaller than the one below the black dashed curve. This means that the number of particles reflected by the finite mass barrier is smaller than this amount in the incident wave packet; consequently, some amount of the wave packet penetrates the barrier and moves there towards $+\infty$ in spite of the fact that its mean energy is smaller than the height of the barrier ($q < 1$). This fact is even better seen in Fig. 6 where the total number of particles in the reflected wave packet is shown as a function

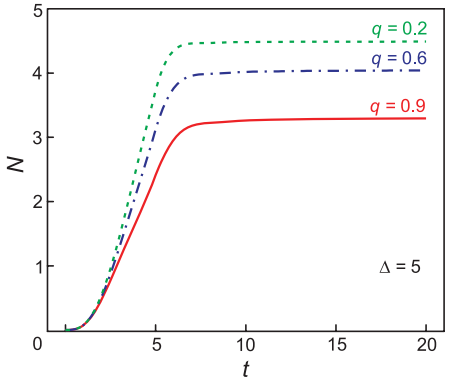

FIG. 6. (Color online) The number of particles in the reflected wave packet as a function of time for different q values in the case when this number for incident wave packet is $N_0 = 5$.

of time. Notice that N is smaller than $N_0 = 5$ (the number of particles in the incident wave packet) in the asymptotic region (for large time t), indicating explicitly that the closer q is to unity the larger the amount of the wave packet that penetrates the barrier.

In Fig. 5(a) we see one more interesting feature. It is a long waving tail that appears due to the above-mentioned degrees of freedom of the barrier. They are excited by the incident wave packet and then radiate the energy even after the incident wave packet disappears. It is remarkable that mathematically this tail follows from the contribution of the cut to the reflected wave function Eq. (33). In the case of large ξ values (which corresponds to the large time t asymptotic) the contribution to the integral is given by the contour edges and leads to the standard power type $1/\xi$ (nonexponential) behavior, that appears in many systems characterized by a continuous spectrum, which for example were discovered in hydrodynamics [23].

VII. REFLECTION AND PENETRATION OF THE GAUSSIAN WAVE PACKET INTO THE MASS BARRIER

Now let us consider the opposite case: the penetration into the mass barrier of a wave packet with a rather soft envelope. We consider the Gaussian wave packet replacing the initial condition Eq. (24) by the following one:

$$\Psi^{(\mathrm{inc})}(x,0) = \frac{1}{\sqrt{2}}\begin{pmatrix}1\\1\end{pmatrix} e^{iqx}\frac{e^{-x^2/2\sigma}}{(\pi\sigma)^{1/4}}. \tag{35}$$

Applying the same scheme as in Sec. IV we present the above wave function as the Fourier integral (25) with the following Fourier transform:

$$f(k) = (4\pi\sigma)^{1/4} e^{-\sigma(q-k)^2/2}. \tag{36}$$

Inserting this Fourier transform into Eq. (25) and replacing the exponent $\exp(ikx)$ by the exponential solution of time dependent Dirac equations (21) and (22) as we did before we obtain the integral representation of the incident Gaussian

wave packet in the free motion region $-\infty < x < 0$,

$$\Psi^{(\mathrm{in})}(x,t) = \frac{\sigma^{1/4}}{2\pi^{3/4}} \begin{pmatrix} 1 \\ 1 \end{pmatrix} \int_C dk e^{-\sigma(q-k)^2/2+ik(x-t)}, \quad (37)$$

its reflected part in the same region,

$$\Psi^{(\mathrm{rfl})}(x,t) = \frac{\sigma^{1/4}}{2\pi^{3/4}} \begin{pmatrix} 1 \\ -1 \end{pmatrix} \int_C dk R(k) e^{-\sigma(q-k)^2/2-ik(x+t)}, \quad (38)$$

and the one penetrated into the barrier ($0 < x < \infty$),

$$\Psi^{(\mathrm{tr})}(x,t) = \frac{\sigma^{1/4}}{2\pi^{3/4}} \int_C dk e^{-iR(k)x} \begin{pmatrix} 1+R(k) \\ 1-R(k) \end{pmatrix} e^{-\sigma(q-k)^2/2+ik(x-t)}. \quad (39)$$

The calculation of these three integrals differs, however, from the calculation of the previous ones in the case of the steep front or rectangular wave packet. The matter is that due to the exponent with momentum k squared the integrand has a more sophisticated singularity at infinity. That is why the integration contour cannot be shifted to ∞, the method applied previously fails, and we have to look for other possibilities to consider those integrals. We demonstrate the method of calculation in the case of the most simple integral Eq. (37) for the incoming wave packet. Analyzing the argument of the single integrand exponent we see that the complex k plane can be divided into four sectors as shown in Fig. 7(a). In two of them, shown by green shadowing, the exponent increase for $|k| \to \infty$. Consequently, the integration contour C has to avoid these two sectors and must be located completely in the two other white sectors. It is evident that going from $-\infty$ to ∞ this integration contour has to cross the saddle point k_0 that is obtained by equating the derivative of the argument of the exponent to zero,

$$\frac{d}{dk}[\sigma(k-q)^2/2 - ik(x-t)]|_{k=k_0} = k_0 - q - i(x-t) = 0, \quad (40)$$

and

$$k_0 = q + i(x-t). \quad (41)$$

The value of the integral can be easily estimated by the saddle-point method. We used the numerical integration over the contour C_0 shown in Fig. 7(b) by the horizontal red solid line. By the way the integral Eq. (37) can be calculated analytically and it reads

$$\Phi(x,t) = \frac{1}{\sqrt{2}} \begin{pmatrix} 1 \\ 1 \end{pmatrix} e^{iq(x-t)} \frac{e^{-(x-t)^2/2\sigma}}{(\pi\sigma)^{1/4}}, \quad (42)$$

which corresponds to the initial condition Eq. (35) that moves with unit velocity to the right, conserving its form, as it should be in the dispersionless free motion region ($-\infty < x < 0$). Thus in the case of the Gaussian wave packet the saddle-point contribution to the integrals is the analog of the contribution of the pole in the case of a rectangular wave packet (or in the pure exponent case).

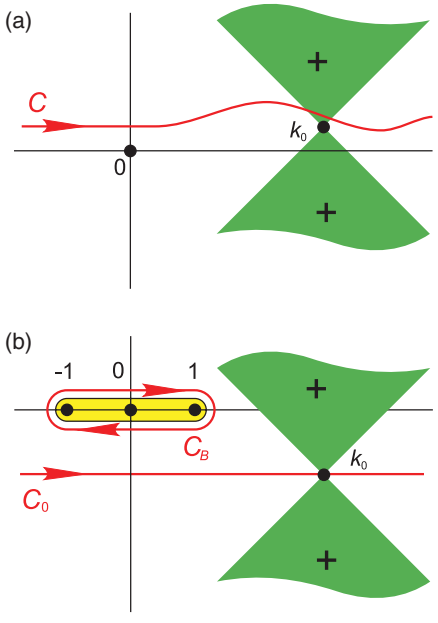

FIG. 7. (Color online) (a) Forbidden sectors in the complex k plane and the integration contour for the calculation of the integrals Eqs. (37)–(39). (b) Transformation of the integration contour in the case $x < t$.

Integrals (38) and (39) are more complicated due to the radical in the function $R(k)$ in the integrands. Because of these radicals there are branching points, and we have to make the cut in the complex k plane connecting them as is shown in Fig. 7(b). Calculating these integrals it is important to check the relative position of the cut and the saddle point that according to Eq. (41) depends on the sign of $(x-t)$. So, if $x > t$ the horizontal contour C_0 crossing the saddle point lays above the cut, and consequently only that contribution has to be taken into account. In the case of $x < t$ as we see in Fig. 7(b) the contour C_0 is located below the cut. In this case the contribution of the cut (namely, the integration over the contour C_B) has to be added. In the case of integrals Eqs. (38) and (39) we performed the integration numerically taking into account the above-mentioned features of the contours.

A typical result for the above barrier reflection of the Gaussian wave packet is shown in Fig. 8. In Fig. 8(a) the reflected wave packet is shown. We see that it differs from the one of the rectangular wave packet or front [see for comparison Figs. 3 and 5(a)]. There is no overshoot or lack of intensity at the edges, and the reflected wave packet conserves more or less its Gaussian form. The matter is that the Gaussian wave packet actually has no leading and trailing edges. The increase (or decrease) of intensity in the Gaussian wave packet is slow, the barrier manages to adjust itself for reflection, and the sophisticated features that we met in the case of rectangular wave-packet reflection are not present. The single reminder of the previously considered reflection of the rectangular wave packet is the small asymmetry of the reflected Gaussian wave packet, some retardation of it as compared with the reflection of the Gaussian wave packet by the hard wall (shown by the thin dashed black curve), and the long waving tail after the reflected wave packet. The wave packet that penetrates the barrier is shown in Fig. 8(b). This differs qualitatively from the rectangular wave-packet case. There are no precursors, and the form of the penetrated wave packet is

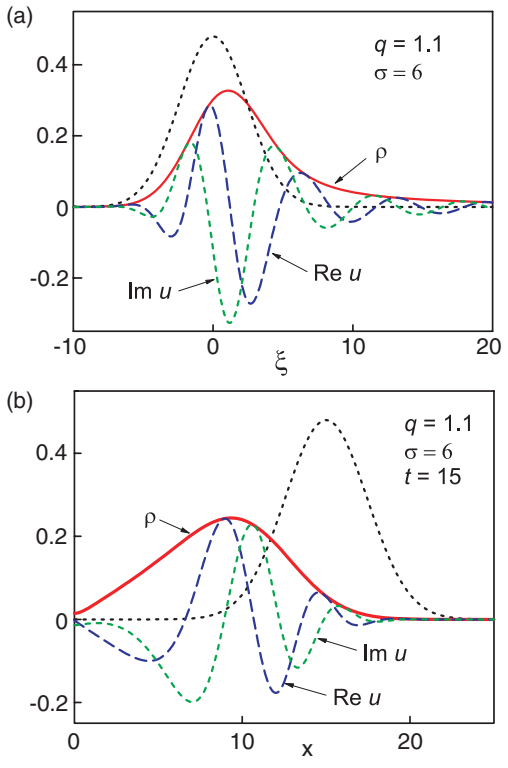

FIG. 8. (Color online) Above the barrier reflection of the Gaussian wave packet: the blue dashed and green dotted curves – the real and imaginary part of wave-function component u (for reflected wave packet it coincides with the component $-v$), and the red solid curve – the density. (a) – reflected wave packet as a function of $\xi = x + t$, the thin dashed black curve – the density of the incident wave packet when it is reflected from the hard wall as in Sec. II. (b) – The wave packet that penetrates the barrier, the thin dashed black curve – the density of the incident wave packet propagating in the absence of the barrier.

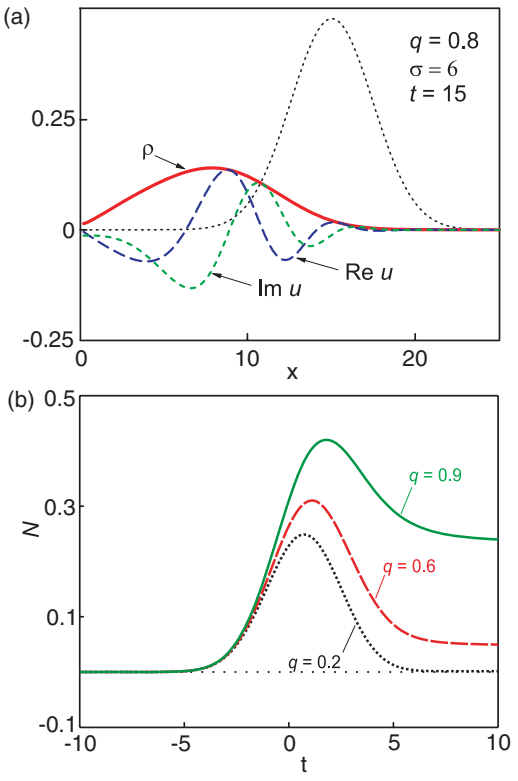

FIG. 9. (Color online) (a) – the same as in 8(b) but for the below the barrier reflection case; (b) – the total number of particles in the barrier (6).

rather close to a Gaussian. It is remarkable that this form is more or less the same even in the case of below the barrier reflection ($q < 1$) as seen in Fig. 9(a), only the amplitude is smaller and the width larger what is caused by the dispersion of the barrier medium. We see no precursors and no formation of an evanescent wave. So, in the case of the below the barrier reflection the penetrated wave packet exhibits qualitatively the same Gaussian form with small asymmetry and this packet is essentially retarded as compared with the motion of the wave packet in the absence of the barrier (shown by the thin dashed black curve) and a rather large spreading that, as it was already mentioned, appears due to the wave dispersion in the barrier. To our mind the retardation of the penetrated wave packet apparently illustrates the problem of the time interval that the wave packet spends in the barrier that was intensively discussed 15 to 20 years ago (see the discussion in Ref. [24]).

In the case of the below the barrier penetration the part of the Gaussian wave packet continues its motion in the barrier towards $+\infty$ as it was in the rectangular wave-packet case, which is clearly seen in Fig. 9(b) where the total number of particles in the barrier is shown as a function of time t. This is clearly demonstrated by the nonzero asymptotic of these values at large t explicitly indicate that. These values increase when the energy q approaches the top of the barrier being essentially larger for short wave packets.

VIII. CONCLUSIONS

We considered a simple 1D model of wave-packet reflection and penetration into a mass barrier. Interesting behavior was already found when considering reflection off a hard wall which is due to the fact that the wave packet is not a point particle. For example we found already reflection before the wave packet reached the wall, there was a compression of the wave packet during reflection, and the width of the wave packet was restored after reflection.

The dependence on the wave-packet shape was discussed by considering two limiting shapes, namely, the rectangular wave packet with sharp leading and trailing edges and the Gaussian wave packet which has a rather soft form.

The most crucial differences of the wave-pack reflection and penetration into the mass barrier with those calculated for standard scattering of exponents were revealed in the case of the rectangular wave packet. Here the dispersion of the electron wave in the barrier showed itself to the full extent. We found different structures moving with different velocities. The leading edge of the front moves with velocity equal to unity because it moves through the unprepared dispersive medium of the barrier. Meanwhile the main piece of the wave packet (or front) moves, however, with the group velocity, which is the reason why it is retarded.

At the leading edge of the reflected front we see some overshoot or failure of some intensity due to the fact that the front itself is a superposition of many exponents that are reflected with different probabilities. In the case of a soft Gaussian wave packet the features of reflection and penetration are quite different. The main difference is the absence of the precursors. The matter is that the soft leading edge of the wave packet prepares the medium of the dispersive barrier gradually, and there is no possibility for the precursor (moving in the unprepared media) to appear. Nevertheless some rudiments of the above features can still be revealed. That is the distortion of the wave-pack form, making its leading edge sharper and the trailing edge more prolonged. Next, we see some retardation of the reflected and penetrated wave packet as compared with the motion in the absence of the barrier.

We also demonstrated that for the Gaussian wave packet in the case when the mean wave-pack energy is lower than the height of the barrier part of the wave packet penetrates into the barrier and moves along it, more or less conserving its shape.

ACKNOWLEDGMENTS

This research was supported by the Flemish Science Foundation (FWO-Vl) and (in part) by the Lithuanian Science Council under Project No. MIP-79/2010.

[1] K. S. Novoselov, A. K. Geim, S. V. Morozov, D. Jiang, Y. Zhang, S. V. Dubonos, I. V. Grigorieva, and A. A. Firsov, Science **306**, 666 (2004).
[2] Y. Zhang, Y. W. Tan, H. L. Stormer, and P. Kim, Nature (London) **438**, 201 (2005).
[3] Y. Zheng and T. Ando, Phys. Rev. B **65**, 245420 (2002).
[4] V. P. Gusynin and S. G. Sharapov, Phys. Rev. Lett. **95**, 146801 (2005).
[5] O. Klein, Z. Phys. **53**, 157 (1929); M. I. Katsnelson, K. S. Novoselov, and A. K. Geim, Nature Phys. **2**, 620 (2006).
[6] P. A. Maksym, Phys. Rev. B **53**, 10871 (1996); S. M. Reinmann and M. Manninen, Rev. Mod. Phys. **74**, 1283 (2002).
[7] Hong-Yi Chen, V. Apalkov and T. Chakraborty, Phys. Rev. Lett. **98**, 186803 (2007); A. Matulis and F. M. Peeters, Phys. Rev. B **77**, 115423 (2008); P. Hewageegana and V. Apalkov, *ibid.* **77**, 245426 (2008); M. Ramezani Masir, A. Matulis, and F. M. Peeters, *ibid.* **79**, 155451 (2009).
[8] G. M. Maksimova, V. Ya. Demikhovskii, and E. V. Frolova, Phys. Rev. B **78**, 235321 (2008); A. Matulis, M. Ramezani Masir, and F. M. Peeters, *ibid.* **83**, 115458 (2011).
[9] J. J. Torres and E. Romera, Phys. Rev. B **82**, 155419 (2010).
[10] A. Chaves, L. Covaci, Kh. Yu. Rakhimov, G. A. Farias, and F. M. Peeters, Phys. Rev. B **82**, 205430 (2010).
[11] G. Giavaras and F. Nori, Appl. Phys. Lett. **97**, 243106 (2010); Phys. Rev. B **83**, 165427 (2011).
[12] D. Gunlycke and C. T. White, Phys. Rev. Lett. **106**, 136806 (2011).
[13] M. Ramezani Masir, A. Matulis, and F. M. Peeters, Phys. Rev. B **84**, 245413 (2011).
[14] J. Lahiri, Y. Lin, P. Bozkurt, I. I. Oleynik, and M. Batzill, Nature Nanotech. **5**, 326 (2010); P. Y. Huang *et al.*, Nature (London) **469**, 389 (2011).
[15] M. Trushin and J. Schliemann, Phys. Rev. Lett. **107**, 156801 (2011).
[16] L. Brillouin, *Wave Propagation and Group Velocity* (Academic Press, New York, 1960), Chap. 1.
[17] E. Schrödinger, Sitzungsber. Preuss. Akad. Wiss. Phys. Math. Kl. **24**, 418 (1930).
[18] W. Zawadzki and T. M. Rusin, J. Phys.: Condens. Matter **23**, 143201 (2011).
[19] G. Giovannetti, P. A. Khomyakov, G. Brocks, P. J. Kelly, and J. van den Brink, Phys. Rev. B **76**, 073103 (2007).
[20] J. D. Jackson, *Classical Electrodynamics* (Wiley, New York, 1962), Chap. 4.7.
[21] J. M. Ziman, *Principles of the Theory of Solids* (Cambridge University Press, Cambridge, 1964), Chap. 8.2.
[22] A. Matulis, Lith. J. Phys. **39**, 435 (1999).
[23] M. H. Ernst and J. R. Dorfman, Physica **61**, 157 (1972).
[24] E. H. Hauge and J. A. Støvneng, Rev. Mod. Phys. **61**, 917 (1989).